Extracellular ATP directly gates a cation-selective channel in rabbit airway ciliated epithelial cells

Alon Korngreen, Weiyuan Ma, Zvi Priel and Shai D. Silberberg*

*Department of Chemistry, *Department of Life Sciences and The Zlotowski Centre for Neuroscience, Ben-Gurion University of the Negev, Beer-Sheva 84105, Israel*

(Received 6 October 1997; accepted after revision 7 January 1998)

1. A membrane conductance activated by extracellular ATP was identified and characterized in freshly dissociated rabbit airway ciliated cells using the whole-cell and outside-out patch configurations of the patch-clamp technique.

2. In solutions designed to maximize currents through voltage-gated calcium channels, there were no indications of voltage-gated Ba^{2+} currents.

3. Extracellular ATP (but not UTP or ADP) activated a membrane conductance which remained activated for several minutes in the presence of ATP. The conductance was permeable to monovalent and divalent cations with approximate relative permeabilities (P) for P_{Ba}: P_{Cs}: P_{TEA} of 4 : 1 : 0·1. Permeability to Cl^- was negligible.

4. Including GDP-β-S in the intracellular solution did not inhibit the effects of ATP, nor did GTP-γ-S irreversibly activate the conductance.

5. In outside-out membrane patches, with GDP-β-S in the pipette solution, ATP activated ion channels which had a chord conductance of approximately 6 pS in symmetrical 150 mM CsCl solutions at −120 mV.

6. Suramin (100 μM) inhibited the whole-cell currents activated by ATP (200 μM) by 93 ± 3 %. Similar effects of suramin were observed on ATP-activated channels in outside-out membrane patches.

7. Extracellular ATP had a priming action on the response to subsequent exposure to ATP. At −40 mV, the time to half-maximal current activation ($t_{½}$) was 46 ± 9 s during the first exposure to 200 μM ATP and decreased to 5 ± 3 s during a second exposure to the same concentration of ATP. The priming action of ATP was not inhibited by including GDP-β-S in the intracellular solution.

8. The initial rate of activation increased with the concentration of ATP, and was voltage sensitive. During the first exposure to 200 μM ATP, $t_{½}$ at +40 mV was 4-fold longer than $t_{½}$ at −40 mV.

9. Half-maximal activation of the conductance shifted from 210 ± 30 to 14 ± 4 μM added ATP when $CaCl_2$ in the extracellular solution was reduced from 1·58 to 0·01 mM. The Hill coefficient for ATP was 1·2 in both solutions.

10. These observations suggest that a form of ATP uncomplexed with divalent cations directly gates an ion channel (P2X receptor) in rabbit airway ciliated cells, which serves as a pathway for Ca^{2+} influx. This purinoceptor may contribute to sustained ciliary activation during prolonged exposures to ATP.

The mucociliary system is responsible for maintaining the airways clean of inhaled particles and pathogens. This immense task is performed by ciliated cells which transport the mucus from the lungs to the upper airways. Ciliary beat frequency (CBF) is strongly regulated by hormones and neurotransmitters via molecular mechanisms which are not fully understood. It is well established, however, that Ca^{2+} is an important mediator, as stimulation of mucociliary activity is correlated with a rise in intracellular Ca^{2+} concentration ($[Ca^{2+}]_i$) (Dirksen & Sanderson, 1989; Villalón, Hinds & Verdugo, 1989; Lansley, Sanderson & Dirksen, 1992; Salathe & Bookman, 1995; Korngreen & Priel, 1996; Levin, Braiman & Priel, 1997).

In various mucociliary systems, extracellular ATP is a potent stimulator of ciliary activity (Ovadyahu, Eshel & Priel, 1988; Villalón *et al.* 1989; Wong & Yeates, 1992; Geary, Davis, Paradiso & Boucher, 1995; Korngreen & Priel, 1996). The receptors and biochemical pathways underlying the effects of ATP on ciliary activity are not well characterized. Cell surface receptors for purines and pyrimidines are classified into two major types: G protein-coupled receptors (P2Y receptors) and ligand-gated ion channels (P2X receptors) (for recent review see Bhagwat & Williams, 1997; North & Barnard, 1997). Most P2Y receptors are coupled to phospholipase C, leading to the formation of inositol 1,4,5-trisphosphate ($InsP_3$), and, thus, to the mobilization of Ca^{2+} from internal stores. However, other cellular effects mediated by P2Y receptors have been reported, including inhibition of adenylate cyclase (Webb *et al.* 1996) and activation of potassium channels (Matsuura, Sakaguchi, Tsuruhara & Ehara, 1996). P2X receptors are ligand-gated cation channels, of which seven functional members have been cloned (for reviews see Bhagwat & Williams, 1997; North & Barnard, 1997). These ATP (and/or other nucleotide)-activated channels, which were first characterized by Benham & Tsien (1987) in vascular smooth muscle, have been identified in several different systems (for reviews see Bean, 1992; Brake & Julius, 1996; Bhagwat & Williams, 1997; North & Barnard, 1997). $P2X_4$, which is relatively insensitive to P2 receptor antagonists such as suramin, is the only functional cloned P2X receptor shown to be present in epithelia (Buell, Lewis, Collo, North & Surprenant, 1996). As yet, however, the role of $P2X_4$ in ATP-induced ciliary activation has not been determined.

In a recent study, the dynamic effects of ATP on CBF and $[Ca^{2+}]_i$ were measured simultaneously in rabbit airway epithelium (Korngreen & Priel, 1996). Extracellular ATP was shown to induce a rapid rise in $[Ca^{2+}]_i$ and in CBF. In the continuous presence of ATP, $[Ca^{2+}]_i$ declined over several minutes to a lower elevated $[Ca^{2+}]_i$ plateau, while CBF remained at a high level throughout the exposure to ATP. The findings of Korngreen & Priel (1996) suggest that the initial rapid rise in both $[Ca^{2+}]_i$ and in CBF results from the mobilization of Ca^{2+} from internal stores while the sustained elevated ciliary activity requires Ca^{2+} influx. Since intracellular Ca^{2+} mobilization by extracellular ATP is mediated by P2Y receptors in many cell types, it is reasonable to assume that the mobilization of Ca^{2+} induced by ATP in the ciliated cells is mediated through at least one type of P2Y receptor. On the other hand, since many of the P2X receptors have been shown to be permeable to Ca^{2+}, it is possible that the ATP-induced Ca^{2+} influx in the ciliated cells is mediated by a P2X receptor. There are, however, other possible pathways for Ca^{2+} influx. Extracellular ATP could indirectly lead to the activation of voltage-gated calcium channels by depolarizing the cell membrane. Alternatively, by binding to P2Y receptors, ATP may indirectly activate calcium-permeable channels via a second messenger system (Naumov, Kiselyov, Mamin, Kaznacheyeva, Kuryshev & Mozhayeva, 1995; Mori, Nishizaki, Kawahara & Okada, 1996; Levin *et al.* 1997).

The present study was designed to pursue the pathway for Ca^{2+} influx activated by extracellular ATP in rabbit airway epithelium, by use of the patch-clamp technique. In freshly dissociated rabbit airway ciliated cells, extracellular ATP was found to activate a cation-selective conductance permeable to Ba^{2+}. The results suggest that the underlying purinoceptor is an ion channel directly gated by a form of ATP which is not bound by divalent cations. The possible implications of these findings for mucociliary regulation are discussed.

METHODS

Isolation of single ciliated cells

Male New Zealand white rabbits (2- to 3-months old) were killed as previously described (Korngreen & Priel, 1996) by gradual exposure to carbon dioxide, followed by exsanguination. Care was taken to slowly increase the gas flow over several minutes to prevent any visual signs of distress. The trachea was removed and the epithelium was surgically separated from the cartilage and cut into pieces of approximately 0·3 cm^2. The tissue was maintained at room temperature in physiological extracellular solution (DPBS) containing (mM): 137 NaCl, 2·7 KCl, 0·9 $CaCl_2$, 0·5 $MgCl_2$, 8 Na_2HPO_4, 1·47 KH_2PO_4, 5 D-glucose, pH 7·4. The epithelium was enzymatically treated for 25 min, at 37 °C, in DPBS supplemented with 13 units ml^{-1} papain (Sigma; lot no. 127F-8075), 1 mg ml^{-1} bovine serum albumin (BSA; Sigma; Fraction V, essentially fatty acid free) and 1 mg ml^{-1} 1,4-dithiothreitol (Merck). Cells were then dispersed by repeated gentle aspiration with a fire-polished Pasteur pipette, concentrated by centrifugation at approximately 2800 *g* for 10 min, and resuspended in DPBS. The isolated cells were transferred to 35 mm tissue culture dishes and used immediately. Single ciliated cells remained active for several hours after isolation and increased CBF in response to extracellular ATP. For unknown reasons, however, the probability of establishing a tight seal between the patch pipette and the membrane of ciliated cells decreased substantially approximately half an hour after cell isolation. Consequently, the epithelium was not all dissociated at the same time, but rather, a piece of epithelium was dissociated before each experiment. In a small number of experiments, part of the tissue was maintained overnight in DPBS at 4 °C and used the next day. No obvious differences in the experimental results, in cell viability or in sensitivity to ATP were observed when cells were used on the next day. Typically, 4–5 experiments could be completed on a successful experimental day.

Solutions and drugs

Solutions were made with highly purified water (NANOpure, Barnstead, Debuque, IA, USA), using chemicals of analytical grade. The standard extracellular solution contained (mM): 151 CsCl, 1·58 $CaCl_2$, 5 Tes, 10 D-glucose, 1 3,4-diaminopyridine (DAP), adjusted to pH 7·4 with CsOH (295–300 mosmol kg^{-1}). The standard pipette solution contained (mM): 155 CsCl, 5 Tes, 0·1 EGTA, 1 MgATP, 0·1 Na_2GTP, 0·037 $CaCl_2$ (0·1 μM Ca^{2+}, estimated by Max Chelator 6.82 (written by Chris Patton, Stanford University, CA, USA), adjusted to pH 7·2 with CsOH (285–290 mosmol kg^{-1}). Deviations from these solutions are noted in the figure legends. The osmolarity of the pipette (intracellular) and bath (extracellular) solutions was set at the above values to prevent the activation of a volume-sensitive chloride conductance found to be expressed in these cells. K_2ATP, MgATP, KADP and $Tris_3UTP$ were purchased

from Sigma. Na_2GTP, Li_4GTP-γ-S and Li_3GDP-β-S were purchased from Boehringer–Mannheim. DAP was purchased from Fluka (Buchs, Switzerland). Tetraethylammonium chloride (TEA-Cl) was purchased from Fluka and Sigma. Suramin was purchased from RBI (Natick, MA, USA). Solutions containing ATP or other nucleotides were prepared fresh each day and the pH of the solution was readjusted.

Estimating the concentrations of the fully ionized (ATP^{4-}) and bound forms of ATP

In ATP-containing solutions in which CsCl is the major salt, Ca^{2+} is the only divalent ion and the pH is adjusted to 7·4, the predominant species of ATP are ATP^{4-}, $HATP^{3-}$, $CsATP^{3-}$ and $CaATP^{2-}$. Other species of ATP are present at low concentrations. While Cs^+ does not bind tightly to ATP^{4-} ($K_{Cs} = 10^{1·06}$ M^{-1}), Cs^+ influences the absolute concentrations of the other species of ATP since it is present at a high concentration relative to the other cations. In the following equations, the effect of Cs^+ on the absolute concentrations of ATP^{4-}, $HATP^{3-}$ and $CaATP^{2-}$ was neglected since the binding constants of Cs^+ to species of ATP other than ATP^{4-} are not known. Therefore, the concentrations of ATP^{4-}, $HATP^{3-}$ and $CaATP^{2-}$ calculated below are approximations of the true concentrations.

The binding constants of ATP to H^+ (K_{H1} and K_{H2}) and of ATP to Ca^{2+} (K_{Ca}) are given by:

$$K_{Ca} = \frac{[CaATP^{2-}]}{[Ca^{2+}][ATP^{4-}]}, \quad (1)$$

$$K_{H1} = \frac{[HATP^{3-}]}{[H^+][ATP^{4-}]}, \quad (2)$$

$$K_{H2} = \frac{[H_2ATP^{2-}]}{[H^+][HATP^{3-}]}. \quad (3)$$

Neglecting other species of ATP present in the solution, one can write:

$$[Ca^{2+}]_{total} = [Ca^{2+}] + [CaATP^{2-}], \quad (4)$$

$$[ATP]_{total} = [ATP^{4-}] + [HATP^{3-}] + [H_2ATP^{2-}] + [CaATP^{2-}]. \quad (5)$$

By substitution it is possible to reduce this set of equations to a second-order polynomial for $[ATP^{4-}]$:

$$0 = (K_{Ca}(1 + K_{H1}[H^+] + K_{H1}K_{H2}[H^+]^2))[ATP^{4-}]^2 + (K_{Ca}([Ca^{2+}]_{total} - [ATP]_{total}) + K_{H1}K_{H2}[H^+]^2 + K_H[H^+] + 1)[ATP^{4-}] - [ATP]_{total}. \quad (6)$$

Binding constants were taken from the National Institute of Standards critical stability constants of metal complexes database (NIST Standard Reference Data, Gaithersburg, MD, USA), and were $10^{6·5}$, 10^4 and $10^{3·9}$ M^{-1} for K_{H1}, K_{H2} and K_{Ca}, respectively. Since the total concentrations of ATP and Ca^{2+} are known, the only unknown parameter in eqn (6) is $[ATP^{4-}]$. In solving eqn (6), only one root was found to be a positive number.

The concentration of $HATP^{3-}$ was calculated from eqn (2), using the concentration of ATP^{4-} derived from eqn (6). The concentration of H_2ATP^{2-} was calculated from eqn (3), using the concentration of $HATP^{3-}$ calculated from eqn (2). The concentration of $CaATP^{2-}$ was calculated from eqn (5) using the concentrations of ATP^{4-}, $HATP^{3-}$ and H_2ATP^{2-} derived above.

Whole-cell current recording

Membrane currents were recorded using the standard whole-cell configuration of the patch-clamp technique (Hamill, Marty, Neher, Sakmann & Sigworth, 1981). The reference electrode was an Ag–AgCl pellet placed in pipette solution and connected via an agar bridge containing 150 mM KCl to the experimental chamber. The agar bridge was maintained in 150 mM KCl solution between experiments to minimize the development of a double bridge (Neher, 1992). Patch pipettes (1–3 MΩ when filled with intracellular solution) were fabricated from borosilicate glass (GC150F-7·5, Clark Electromedical Instruments, Reading, UK), coated with Sylgard 184 (Dow Corning) and fire polished shortly before use. Tight seals (> 10 GΩ) were obtained with DPBS as the external solution by pressing the pipette against a cilia-free patch of membrane until the resistance of the pipette doubled, followed by gentle suction. Occasionally, tight seal formation was facilitated by applying −40 mV to the patch pipette. The membrane underlying the pipette was then ruptured by further suction. The average cell capacitance of the ciliated cells was 15 ± 0·3 pF (mean ± S.E.M.; $n = 122$) and the series resistance ranged from 4·5 to 37 MΩ, with a mean (± S.E.M.) of 11 ± 0·5 MΩ. Capacitive currents were electronically compensated. Series resistance was not compensated in most experiments, since the currents activated by ATP were small (less than 500 pA). Once the whole-cell configuration was established, the cell was continuously superfused with the desired extracellular solutions via a gravity-fed perfusion system. The outlet of the perfusion tube was placed approximately 300 μm away from the cell under investigation. The bathing solution was changed using a Teflon rotary valve which selected among one of six reservoirs. The perfusion time from the rotary valve to the outlet of the tube (dead time for solution change) was 16–18 s. The perfusion time from the reservoirs through the entire length of the tubing was 50–55 s. The continuous perfusion of the cell prevented fluctuations in the concentration of ATP due to degradation of ATP by ectonucleotidases, and prevented the possible build-up of degradation products such as ADP. Liquid junction potentials were determined by adjusting the bath potential to zero with a patch pipette containing internal solution placed in internal solution, and then measuring the bath potential in each of the external solutions (Neher, 1992). Liquid junction potentials were not corrected since variations in liquid junction potentials were at most 1·5 mV. All measurements were at room temperature (18–22 °C).

Data acquisition and analysis

Experiments were initiated at least 5 min after establishing the whole-cell configuration to allow equilibration of the cytosol with the pipette solution. Membrane currents were recorded under voltage clamp using an Axopatch 200A or 200B patch-clamp amplifier (Axon Instruments). Stable recordings were typically maintained for 20–30 min. Membrane currents were low-pass filtered using an 8-pole Bessel filter (Frequency Devices, Haverhill, MA, USA) in series with the integral 4-pole Bessel filter of the patch-clamp amplifier and stored on VCR tape for subsequent analysis (VR-10B, Instrutech). Membrane currents were also digitized on-line using a Digidata 1200 interface board and pCLAMP 6.03 software (Axon Instruments). The sampling frequency was set to at least two times the corner frequency of the low-pass filter. SigmaPlot 2.0 scientific software (Jandel Scientific, San Rafael, CA, USA) was used for non-linear curve fitting. Experimental results were consistently observed in cells from two or more animals, hence all the results for a particular experiment were pooled and displayed as means ± S.E.M.; groups were compared with Student's t test.

Single-channel current recording

Single-channel currents were recorded in the outside-out patch configuration of the patch-clamp technique (Hamill *et al.* 1981). The experimental set-up was the same as that used for whole-cell

recordings. To anchor the cells to the bottom of the experimental chamber, the dissociated cells were placed on glass coverslips coated with concanavalin A (Sigma), as described by Kim, Dirksen & Sanderson (1993). Single-channel currents were low-pass filtered at 50 Hz and digitized at 100–500 Hz. The currents were further amplified using a custom-made amplifier and residual line frequency noise was removed with a Hum Bug noise eliminator (Quest Scientific, Vancouver, Canada). Occasional large brief noise spikes were visually identified and removed from the current traces. In the majority of the outside-out patch experiments, the pipette solution contained 0·2 mM GDP-β-S and no added GTP to prevent the activation of G protein-mediated ion channels.

Calculating the permeability of Ba^{2+} over Cs^+

When the extracellular solution contains a permeant monovalent ion (for example, TEA^+) and a permeant divalent ion (for example, Ba^{2+}), and the intracellular solution contains only a permeant monovalent cation (for example, Cs^+), the relationship between the reversal potential (V_{rev}) and the relative ion permeabilities predicted by the Goldman–Hodgkin–Katz equation is described by (Lewis, 1979):

$$V_{rev} = \frac{RT}{F}\ln\left(\frac{P_{TEA}\gamma_{TEA}[TEA]_o + (4/(1+e^{V_{rev}F/RT}))P_{Ba}\gamma_{Ba}[Ba]_o}{P_{Cs}\gamma_{Cs}[Cs]_i}\right), \quad (7)$$

where R is the universal gas constant, T is the absolute temperature, F is Faraday's constant, P_{TEA}, P_{Ba} and P_{Cs} are the permeabilities to TEA^+, Ba^{2+} and Cs^+, respectively, γ_{TEA}, γ_{Ba} and γ_{Cs} are the activity coefficients of TEA^+, Ba^{2+} and Cs^+ , respectively, $[TEA]_o$and $[Ba]_o$ are the concentrations of TEA^+ and Ba^{2+} in the extracellular solutions, respectively, and $[Cs]_i$ is the concentration of Cs^+ in the intracellular solution.

Since the reversal potential (V_{rev}) appears on both sides of the equation, V_{rev} was extracted by solving first for $e^{V_{rev}F/RT}$ and then solving the resulting cubic equation to obtain:

$$V_{rev} = \frac{RT}{F}\ln\left\{\left(\frac{P_{TEA}}{P_{Cs}}\frac{\gamma_{TEA}[TEA]_o}{\gamma_{Cs}[Cs]_i} - 1 + \sqrt{\left(1+\frac{P_{TEA}}{P_{Cs}}\frac{\gamma_{TEA}[TEA]_o}{\gamma_{Cs}[Cs]_i}\right)^2 + 16\frac{P_{Ba}}{P_{Cs}}\frac{\gamma_{Ba}}{\gamma_{Cs}}\frac{[Ba]_o}{[Cs]_i}}\right)\Big/2\right\}. \quad (8)$$

P_{TEA}/P_{Cs} was calculated in independent experiments (see Results), hence the permeability ratio P_{Ba}/P_{Cs} could be quantified by comparing the reversal potentials measured experimentally at different Ba^{2+} concentrations to the reversal potentials predicted from eqn (8). The estimated permeability ratio P_{Ba}/P_{Cs} depends on the choice of activity coefficients for these ions (γ_{Ba} and γ_{Cs}). In mixed electrolyte solutions, each salt influences the activity coefficient of the other electrolytes in the solution. However, in mixed solutions of total ionic strength up to 0·2 M, it can be assumed that the activity of an individual ion is determined solely by the ionic strength of the solution, and not by the chemical nature of the other ions in the solution (Shatkay, 1968). Hence, the activity coefficients for CsCl and $BaCl_2$ (Robinson & Stokes, 1959) and the activity coefficient for TEA-Cl (Lindenbaum & Boyd, 1964) were adjusted for total ionic strength, and used to estimate the activity coefficient of Cs^+, Ba^{2+} and TEA^+, respectively. Various assumptions have been made in order to estimate the activity coefficient of a divalent cation (γ_{++}) from the mean activity coefficient of the salt ($\gamma_{\pm}$) in mixed solutions (see Butler, 1968). In the present study, two conceptually different assumptions were used, $\gamma_{++} = \gamma_{\pm}$ (Shatkay, 1968) and $\gamma_{++} = (\gamma_{\pm})^2$ (Butler, 1968), and the resulting estimates of P_{Ba}/P_{Cs} were compared (see Results).

RESULTS

A voltage-insensitive conductance is activated by extracellular ATP

In rabbit airway ciliated cells, extracellular ATP causes both the release of Ca^{2+} from internal stores and Ca^{2+} influx from the extracellular solution (Korngreen & Priel, 1996). The aim of the present study was to identify the pathway for Ca^{2+} influx activated by extracellular ATP by recording whole-cell currents. In order to measure currents that would be carried through calcium channels, the solutions used in the initial experiments were designed to both abolish K^+ currents and to prevent the development of volume-sensitive Cl^- currents found to be expressed in these cells (see Methods). The extracellular (bath) solution also contained 10 mM Ba^{2+}, an ion that typically carries larger currents through calcium channels than Ca^{2+} itself (Hille, 1992).

The results presented in this study are based on experiments performed on more than 150 ciliated cells. In these experiments, extracellular ATP consistently activated a membrane conductance in a reversible manner. This is shown in Fig. 1*A*, which presents a continuous whole-cell current trace recorded at a holding potential of −60 mV. The addition of 200 μM K_2ATP in the extracellular solution activated an inward current. The current activated by ATP reached half-maximal activation after 4 s and deactivated to half the maximal current within 6 s, upon removal of the ATP. In all the experiments it was observed that the response to the first application of ATP was slower than the response to subsequent applications of ATP. This priming effect of ATP (not shown in Fig. 1*A*) is presented in detail in a later section.

The current activated by ATP gradually declined with time in the continuous presence of ATP. This run-down of the ATP-activated current (shown in Fig. 5) was dependent on the concentration of ATP. Hence, in most experiments K_2ATP was used at a concentration of 200 μM , since this concentration was found to induce sizable currents which typically exhibited a moderate rate of run-down (Fig. 1*A*).

The voltage dependence of the ATP-activated conductance was investigated by applying voltage steps from a holding potential of −60 mV to potentials ranging from −70 to +30 mV. In comparison to the control currents (Fig. 1*B*), the addition of 200 μM K_2ATP in the extracellular solution increased both the inward currents induced by steps to negative membrane potentials and the outward currents induced by steps to positive membrane potentials (Fig. 1*C*). The net current activated by ATP (Fig. 1*D*) was determined by subtracting the current under control conditions (Fig. 1*B*) from the current in the presence of ATP (Fig. 1*C*). Figure 1*E* plots the net current activated by ATP for a range of membrane potentials. Each point represents the current density, defined as the current divided by the cell capacitance, averaged from five experiments. The relatively sustained currents in response to voltage steps, with no

time-dependent changes in amplitude (Fig. 1*D*), and the approximately linear relationship between current and voltage in Fig. 1*E* suggest that ATP activated a voltage-insensitive conductance.

Under control conditions, over a wide range of voltages, step changes in voltage gave rise to relatively sustained currents with no time-dependent changes in amplitude (Fig. 1*B*). This suggests that ciliated cells freshly dissociated from rabbit airway do not express voltage-gated calcium channels. Similar results of the type shown in Fig. 1*B* were observed in six of six additional experiments. The absence of voltage-gated barium currents in the ciliated cells is in agreement with earlier observation that calcium channel blockers, such as verapamil and diltiazem, did not alter Ca^{2+} influx induced by extracellular ATP and had little effect on ciliary motility in rabbit airway epithelium (Korngreen & Priel, 1996). Thus, control of Ca^{2+} entry in ciliated cells from rabbit airway appears different from *Paramecium* and other ciliated protozoans, where Ca^{2+} influx occurs primarily through voltage-dependent calcium channels (reviewed by Tamm, 1994).

Cs^+ and TEA^+ permeate the conductance activated by ATP

In the experiments summarized in Fig. 1*E*, the net current activated by ATP reversed at approximately −20 mV. Since none of the major ions in the solutions had a Nernst equilibrium potential (zero current potential) close to −20 mV, most probably more than one ion species permeated the conductance activated by ATP. The ionic selectivity of the current activated by ATP was, therefore, investigated by ion substitutions. The simplest way to estimate ionic permeability ratios is to have only one permeant ion on each side of the membrane (Hille, 1992). However, as will be shown in a later section, extracellular solutions containing

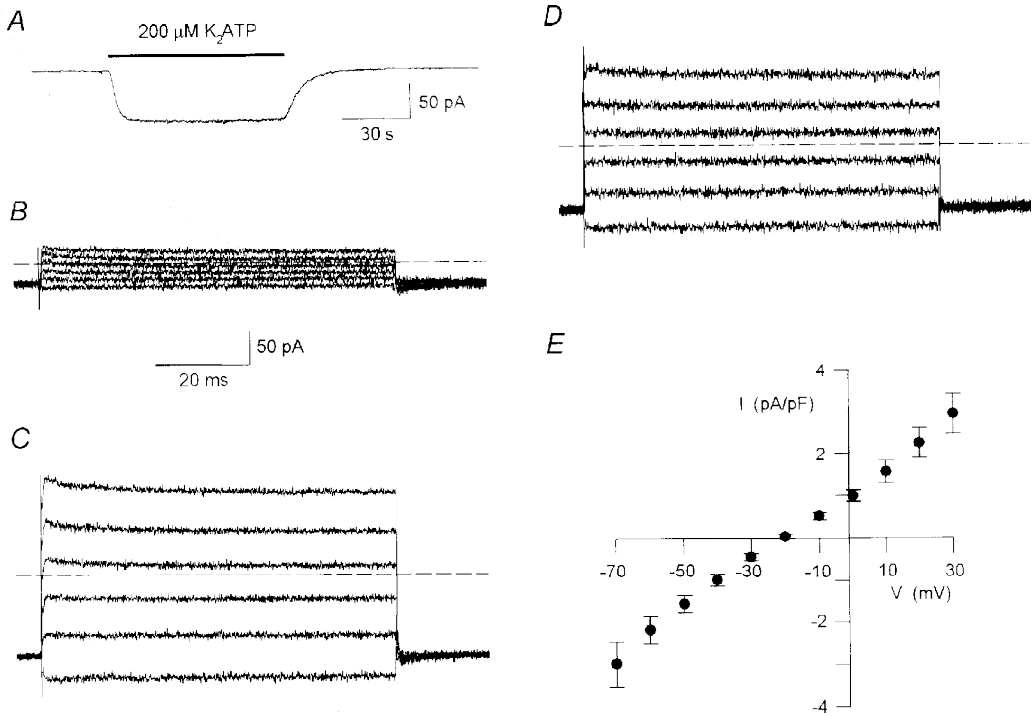

Figure 1. Extracellular ATP activated a voltage-insensitive conductance

A, continuous whole-cell current trace recorded at a holding potential of −60 mV. The cell was exposed to K_2ATP (200 μM) during the time indicated by the bar. The current activated by ATP reached half-maximal activation after 4 s and deactivated to half the maximal current within 6 s, upon removal of the ATP. Not shown is the response to the first application of ATP, which was substantially slower. The extracellular (bath) solution contained (mM): 140 TEA-Cl, 10 $BaCl_2$, 10 D-glucose, 1 DAP, 5 Tes, adjusted to pH 7·4 with TEA-OH. Standard intracellular (pipette) solution. Digitized at 100 Hz, filtered at 50 Hz. Cell capacitance, 16 pF; series resistance, 5 MΩ. *B* and *C*, whole-cell currents in response to voltage steps from a holding potential of −60 mV in the absence (*B*) and presence (*C*) of extracellular K_2ATP (200 μM). Voltage steps were between −70 and +30 mV at 20 mV increments. Dashed lines indicate the zero current level. Same solutions as in *A*. Digitized at 20 kHz, filtered at 5 kHz. Cell capacitance, 15·5 pF; series resistance, 4·5 MΩ. *D*, net currents activated by ATP, determined by subtracting the control current traces (*B*) from the traces in the presence of ATP (*C*). The zero current level is indicated by a dashed line. The calibration bar in *B* is also for *C* and *D*. *E*, mean (± S.E.M.) net current activated by ATP in response to voltage steps at 10 mV increments, averaged from 5 experiments of the type shown in *D*. The currents were normalized to cell size by dividing the currents for each cell by the cell capacitance (current density).

only $BaCl_2$ or only $CaCl_2$ could not be used, since a form of ATP which is uncomplexed with divalent cations activated the conductance. Hence, the relative permeabilities of Cs^+ and TEA^+ were determined first and used to estimate the relative permeabilities of Ba^{2+} and Cs^+ (see Methods).

In the experiments designed to determine the relative permeabilities of Cs^+ and TEA^+, the pipette contained 155 mM CsCl while the bath contained either 151 mM CsCl or different combinations of CsCl and TEA-Cl. In each extracellular solution, the osmolarity of the solution and the concentration of Cl^- were kept constant by equimolar substitution of CsCl with TEA-Cl. Figure 2*A* shows net whole-cell currents activated by ATP in response to voltage ramps measured in extracellular solutions containing different concentrations of CsCl, as indicated by the current traces. Since the concentration of Cl^- was the same for each of the extracellular solutions, the observed shifts in the zero current potential (reversal potential) with changes in the cation composition indicate that ATP activated a cation-permeable conductance. Furthermore, in five experiments, the extracellular Cl^- was substituted with a large anion (methanesulphonate) with no obvious shift in the reversal potential, indicating that the permeability of the ATP-activated conductance to Cl^- was negligible (data not shown).

Figure 2*B* summarizes the dependence of the reversal potential on the concentration of extracellular Cs^+, determined in experiments of the type shown in Fig. 2*A*. The non-linear dependence of the reversal potential on the log concentration of extracellular Cs^+ indicates that TEA^+ also permeated the conductance activated by ATP. The permeability ratio, P_{TEA}/P_{Cs}, was quantified by comparing the reversal potentials (V_{rev}) measured experimentally to the reversal potentials predicted by the Goldman–Hodgkin–Katz equation:

$$V_{rev} = \frac{RT}{F} \ln\left(\frac{P_{Cs}\gamma_{Cs}[Cs]_o + P_{TEA}\gamma_{TEA}[TEA]_o}{(P_{Cs}\gamma_{Cs}[Cs]_i}\right), \quad (9)$$

where R is the universal gas constant, T is the absolute temperature, F is Faraday's constant, P_{Cs} and P_{TEA} are the permeabilities to Cs^+ and TEA^+, respectively, γ_{Cs} and γ_{TEA} are the activity coefficients of Cs^+ and TEA^+, respectively, $[Cs]_o$ and $[TEA]_o$ are the concentrations of Cs^+ and TEA^+ in the extracellular solution, respectively, and $[Cs]_i$ is the concentration of Cs^+ in the intracellular solution. The activities of Cs^+ and TEA^+ were calculated using two different assumptions (see Methods). Both assumptions resulted in a similar permeability ratio for P_{TEA}/P_{Cs}, since the activity coefficients of CsCl and TEA-Cl are negligibly

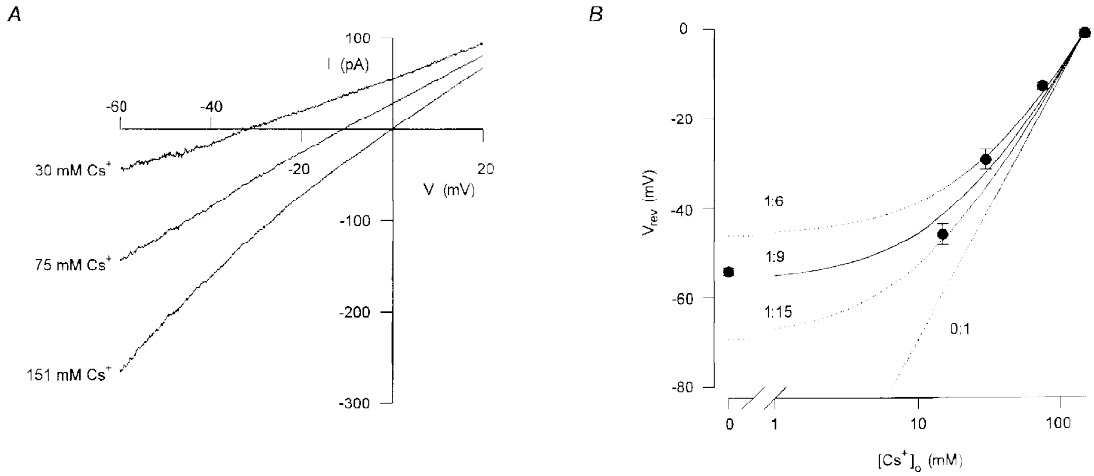

Figure 2. The conductance activated by ATP was cation selective with Cs^+ being 9-fold more permeant than TEA^+

A, mean whole-cell currents activated by extracellular ATP in response to voltage ramps in extracellular solutions containing either 151 mM CsCl or different combinations of CsCl and TEA-Cl. In each extracellular solution, the net current activated by ATP was assessed by subtracting the current recorded under control conditions from the current recorded in the presence of 200 μM ATP. The concentrations of Cs^+ in the extracellular solution are indicated by each current trace. The osmolarity of the solution was maintained the same by equimolar substitution of CsCl with TEA-Cl. The extracellular solution also contained (mM): 5 Tes, 10 D-glucose, 1 DAP and 0·1 $BaCl_2$ which was found to be required for the stability of the recordings. Five to eight consecutive current traces were averaged in each experimental condition. Digitized at 1 kHz, filtered at 0·5 kHz. Cell capacitance, 19 pF; series resistance, 5·5 MΩ. *B*, the reversal potential of the current activated by ATP had a non-linear dependency on the log concentration of Cs^+. The mean (± S.E.M.) reversal potentials of the current activated by ATP in extracellular solutions containing different concentrations of Cs^+ (symbols) were averaged from 5–15 experiments of the type shown in *A*. The relative permeability of TEA^+ and Cs^+(P_{TEA}/P_{Cs}) was estimated to be 1 : 9 from eqn (9) in Results (continuous line). Permeability ratios of 1 : 6, 1 : 15 and 0 : 1 are also shown (dotted lines).

different (0·752 and 0·750, respectively, for 0·1 M solution at 25 °C). A permeability ratio for P_{TEA}/P_{Cs} of 1 : 9 was estimated from eqn (9) and is shown as a continuous line in Fig. 2*B*. For comparison, predicted reversal potentials assuming permeability ratios for P_{TEA}/P_{Cs} of 1 : 6, 1 : 15, and 0 : 1 are also shown (dotted lines).

Ba^{2+} also permeates the conductance activated by ATP

To assess whether Ba^{2+} can also permeate the conductance activated by ATP, the effect of changes in extracellular Ba^{2+} on the ATP-activated currents was examined. Figure 3*A* shows a continuous whole-cell current trace recorded at a holding potential of −50 mV, under the same experimental conditions as in Fig. 1 (i.e. intracellular CsCl and extracellular TEA-Cl and $BaCl_2$). Extracellular ATP (200 μM) activated an inward current which decreased when the concentration of $BaCl_2$ in the extracellular solution was lowered from 10 mM to 0·1 mM. Switching back to 10 mM $BaCl_2$ then restored the current. The reduction in inward current induced by lowering the extracellular concentration of $BaCl_2$ is consistent with Ba^{2+} permeating the channels activated by ATP.

The effect of changes in external Ba^{2+} on the reversal potential was examined by applying voltage ramps, in the presence and absence of extracellular ATP. The ATP-activated (difference) currents for one such experiment are shown in Fig. 3*B*. Decreasing external $BaCl_2$ from 20 to 10 to 0·1 mM shifted the reversal potential from −4 to −19 to −51 mV, respectively, indicating that Ba^{2+} is permeant. Figure 3*C* summarizes the dependence of the reversal potential on the concentration of extracellular Ba^{2+}, determined in experiments of the type shown in Fig. 3*B*. A permeability ratio for P_{Ba}/P_{Cs} of 4 : 1 was estimated from eqn (8) (continuous line in Fig. 3*C*) when the activity coefficient of Ba^{2+} (γ_{++}) was assumed to be equal to the mean activity coefficient of $BaCl_2$ ($\gamma_{\pm}$) (see Methods). For comparison, predicted reversal potentials assuming permeability ratios for P_{Ba}/P_{Cs} of 6 : 1 and 2 : 1 are also shown (dotted lines). If γ_{++} was assumed to be equal to $(\gamma_{\pm})^2$, then P_{Ba}/P_{Cs} was estimated to be 6 : 1. Regardless of the method for estimating the activity coefficient of the ions, the results shown in Fig. 3*C* clearly indicate the conductance activated by ATP is more permeable to Ba^{2+} than to Cs^+.

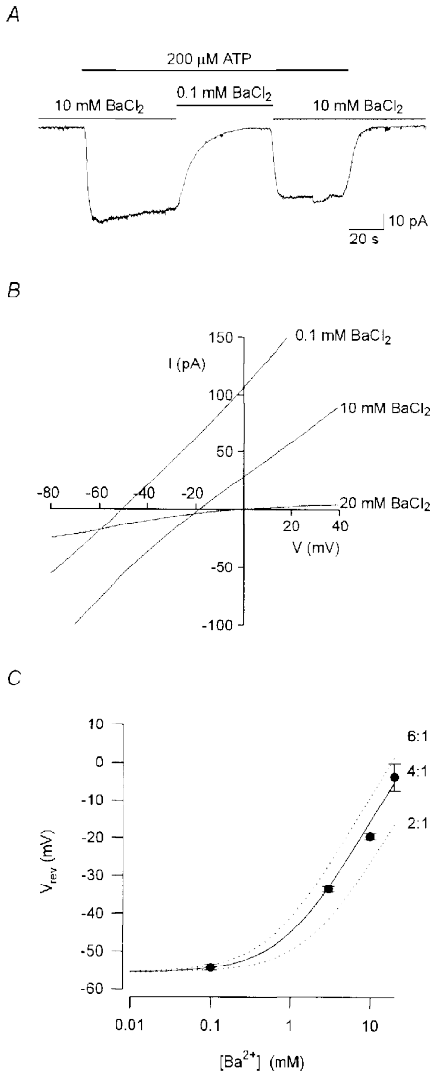

Figure 3. The conductance activated by ATP was more permeable to Ba^{2+} than to Cs^+

A, continuous whole-cell current trace recorded at a holding potential of −50 mV, from a cell exposed to extracellular ATP (200 μM) for the duration indicated by the topmost bar. The extracellular solutions contained either 140 mM TEA-Cl and 10 mM $BaCl_2$ or 151 mM TEA-Cl and 0·1 mM $BaCl_2$, as indicated by the bars above the current trace. Both extracellular solutions contained in addition (mM): 5 Tes, 10 D-glucose and 1 DAP, adjusted to pH 7·4 with TEA-OH. Standard intracellular solution. Digitized at 100 Hz, filtered at 50 Hz. Cell capacitance, 17 pF; series resistance, 35 MΩ. *B*, average whole-cell currents activated by extracellular ATP in response to voltage ramps in extracellular solutions containing either 20, 10 or 0·1 mM $BaCl_2$. Ten consecutive current traces were averaged in each experimental condition. Digitized at 1 kHz, filtered at 0·5 kHz. Cell capacitance, 15·5 pF; series resistance, 26 MΩ. Same solutions as in *A*. The solution with 20 mM $BaCl_2$ included 121 mM TEA-Cl. *C*, mean (± S.E.M.) reversal potentials of the current activated by ATP in extracellular solutions containing different concentrations of $BaCl_2$ (symbols), averaged from 3–15 experiments of the type shown in *B*. The relative permeability of Ba^{2+} and Cs^+ (P_{Ba}/P_{Cs}) was estimated from eqn (8) in Methods to be 4 : 1 (continuous line). Permeability ratios of 6 : 1 and 2 : 1 are also shown (dotted lines).

The conductance activated by ATP requires priming for rapid activation

As mentioned above, ATP was found to have a priming action on the response to subsequent exposure to ATP. Figure 4*A* shows a continuous whole-cell current trace at a holding potential of −40 mV, recorded in CsCl solutions, from a cell not previously exposed to extracellular ATP. The addition of ATP (200 μM) slowly activated an inward current. The current activated by ATP reached half-maximal activation after 43 s and deactivated to half the maximal current within 8 s, upon removal of the ATP. In contrast, activation was markedly faster during a second application of ATP, reaching half-maximal activation within 4 s. In nine experiments of the type shown in Fig. 4*A*, the time to half-maximal current activation ($t_{½}$) was 46 ± 9 s during the first exposure to 200 μM ATP and decreased to 5 ± 3 s during a second exposure to the same concentration of ATP (Fig. 4*B*, open and filled columns at 200 μM ATP).

For Fig. 4*A*, the second application of ATP was 65 s after the first. In four experiments, accelerated activation by ATP was still observed 15 min after the first two applications of ATP. In these four experiments, the $t_{½}$ was 54 ± 20 s for the first application of ATP, 7 ± 1 s for the second application of ATP and 11 ± 3 s for a third application of ATP 15 min later. On the other hand, if during the first application of ATP the nucleotide was removed before the current fully developed, a subsequent application of ATP still produced a slowly rising current rather than a rapidly

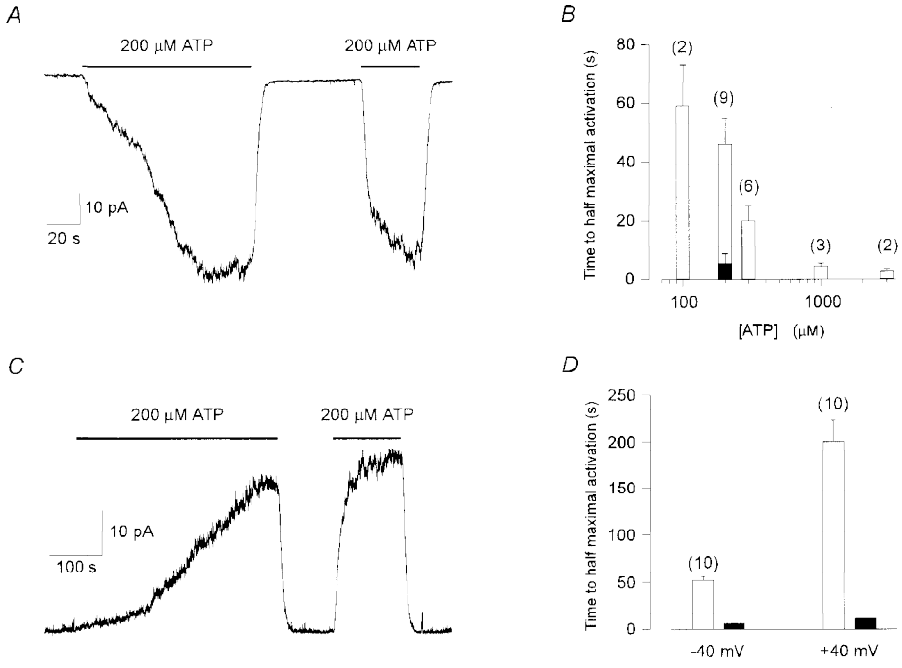

Figure 4. Extracellular ATP had a priming action on the response to subsequent exposures to ATP

A, continuous whole-cell current trace recorded at a holding potential of −40 mV, from a cell not previously exposed to ATP. Extracellular ATP was applied twice (indicated by the bars). Half-maximal current activation was 43 s during the first exposure to ATP and 4 s during the second exposure to ATP. The current deactivated by 50% within 8 s and 7·5 s upon removal of the first and second applications of ATP, respectively. Standard intracellular and extracellular solutions. Digitized at 100 Hz, filtered at 50 Hz. Cell capacitance, 13 pF; series resistance, 15 MΩ. *B*, the mean (± S.E.M.) $t_{½}$ during the first exposure to ATP (□) decreased as the concentration of ATP was increased. The number of experiments at each concentration of ATP is indicated above each bar. ■, average $t_{½}$ during a second exposure to 200 μM ATP. *C*, continuous whole-cell current trace recorded at a holding potential of +40 mV, from a cell not previously exposed to ATP. Note the difference in time scales between *A* and *C*. Extracellular ATP (200 μM) was applied twice (indicated by the bars). Half-maximal current activation was 252 s during the first exposure to ATP and 10 s during the second exposure to ATP. The current deactivated by 50% within 10 s and 9 s upon removal of the first and second applications of ATP, respectively. Standard intracellular and extracellular solutions, except that the pipette solution did not include GTP. Digitized at 100 Hz, filtered at 50 Hz. Cell capacitance, 7 pF; series resistance, 10 MΩ. *D*, the mean (± S.E.M.) $t_{½}$ during the first exposure to ATP (□) is significantly ($P < 0{\cdot}00001$) longer at a holding potential of +40 mV (200 ± 23 s) in comparison to −40 mV (52 ± 4 s). Ten experiments were performed at each voltage (indicated above each column). ■, average $t_{½}$ during a second exposure to 200 μM ATP at either +40 mV (12 ± 2 s) or −40 mV (6 ± 2 s). Same solutions as in *C* for both membrane potentials.

rising current (data not shown). These observations suggest that exposure to ATP (or a breakdown product of ATP present in the solutions) has a long-lasting priming effect on the rate of rise of the conductance activated by ATP.

The priming effect of ATP was found to be significantly ($P < 0{\cdot}00001$) slower at +40 mV. Figure 4*C* presents a continuous whole-cell current trace recorded in CsCl solutions, at a holding potential of +40 mV, from a cell not previously exposed to extracellular ATP (note the difference in time scale in comparison to Fig. 4*A*). The $t_{½}$ induced by ATP (200 μM) was 252 s for the first application of ATP and decreased to 10 s for the second application of ATP. In ten experiments of the type shown in Fig. 4*C*, the $t_{½}$ during the first and second exposures to 200 μM ATP were 200 ± 23 s and 12 ± 2 s, respectively (Fig. 4*D*, open and filled columns, at +40 mV). In comparison, at −40 mV, using the same extracellular and intracellular solutions (see legend to Fig. 4), the $t_{½}$ during the first and second exposures to ATP were 52 ± 4 s and 6 ± 2 s, respectively (Fig. 4*D*, open and filled columns, at −40 mV).

The $t_{½}$ during the second exposures to ATP was significantly ($P < 0{\cdot}0001$) longer at +40 mV in comparison to −40 mV (Fig. 4*D*, filled columns). The mechanism underlying the longer $t_{½}$ during the second exposures to ATP at +40 mV was not further investigated, though it could result from a voltage dependence of receptor activation, from less run-down at positive potentials, or due to incomplete priming during the first exposure to ATP.

In the experiments shown in Fig. 4*A* and *C* the current activated by the first application of ATP appeared to develop in two steps (see also Figs 5*A* and 6*A*). After priming, the current also appeared to activate in two steps: an initial fast activation step followed by a slower activation step (Figs 4*A*

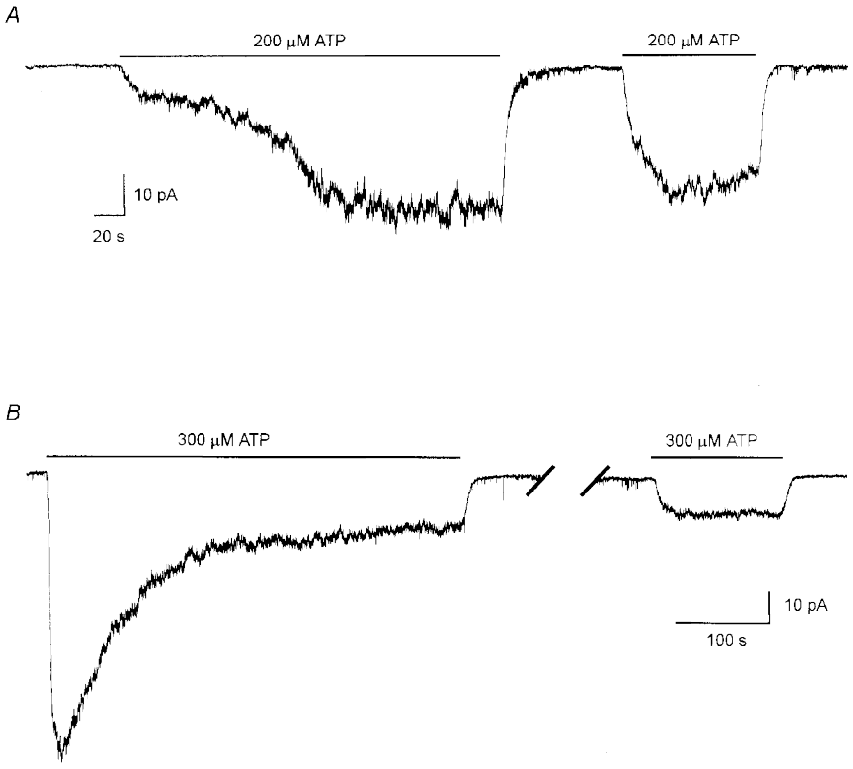

Figure 5. G proteins did not mediate current activation by extracellular ATP nor the priming effect of ATP

A, the priming effect of extracellular ATP was not prevented by including GDP-β-S (200 μM) in the pipette solutions in place of GTP (200 μM). Continuous whole-cell current trace recorded at a holding potential of −40 mV. The cell was exposed to ATP (200 μM) at the times indicated by the bars. Half-maximal current activation was 107 s during the first exposure to ATP and 14 s during the second exposure to ATP. The current deactivated by 50% within 3·5 and 3 s upon removal of the first and second applications of ATP, respectively. Digitized at 100 Hz, filtered at 50 Hz. Cell capacitance, 14 pF; series resistance, 6 MΩ. *B*, the current activated by extracellular ATP was not irreversibly activated by including GTP-γ-S (200 μM) in the pipette solution in place of GTP. Run-down of the current activated by ATP was also not prevented by GTP-γ-S. Continuous current trace, recorded at a holding potential of −40 mV. Extracellular ATP (300 μM) was applied twice, indicated by the bars. The break in the current trace represents 10 min during which the cell was not exposed to ATP. The first (priming) application of ATP is not shown. Digitized at 100 Hz, filtered at 50 Hz. Cell capacitance, 12 pF; series resistance, 9 MΩ.

and *C*, 5 and 6*A*). The mechanisms underlying the complex kinetics of activation, which were consistently observed, were not further studied.

The dependence of the initial rate of current activation on the concentration of extracellular ATP was also examined. Figure 4*B* shows the average $t_{½}$ during the first exposure to different concentrations of ATP (open columns), and the average $t_{½}$ for a second exposure to 200 μM ATP (filled column). The rate of current activation during the first exposure to ATP increased as the concentration of ATP increased. This observation suggests that the channels were accessible for activation and, thus, that the slow activation was probably not due to the insertion of additional channels. The effects of membrane potential on the priming process (Fig. 4*B* and *C*) strongly suggest that the slow rate of current activation by ATP is a biological phenomenon.

The effects of extracellular ATP are not mediated by G proteins

In the previous section it was shown that ATP both activated and primed a membrane conductance and that the rate of activation was complex, and depended on the membrane potential and on the concentration of applied ATP. The priming effect of extracellular ATP could have resulted from direct modulation of the ion-conducting pathway or could have been mediated by a second messenger system. Since adenosine receptors (P1 receptors) and several of the ATP receptors (P2 receptors) regulate cellular functions through G protein-coupled pathways (Fredholm *et al.* 1994; Harden, Boyer & Nicholas, 1995), the possible involvement of G proteins in the priming process was examined.

If a G protein-mediated pathway is involved in the priming process, the time course of current activation by ATP would most likely be independent of earlier applications of ATP, once the G proteins were inhibited. The priming effect of ATP was, therefore, investigated using intracellular solutions containing (in place of GTP) a non-hydrolyzable analogue of GDP (GDP-β-S) which inhibits G proteins. ATP was applied to the cells at least 5 min after establishing the whole-cell configuration to allow the diffusion of GDP-β-S from the patch pipette into the cell. Figure 5*A* shows that GDP-β-S did not prevent the priming effect of ATP since a second application of ATP (200 μM), at a holding potential of −40 mV, activated the current with a time course which was similar to that observed with GTP in the intracellular solution (Fig. 4*A*). For this particular example, which had an unusually slow priming for a holding potential of −40 mV, the $t_{½}$ was 109 and 8 s for the first and second exposures to ATP, respectively. In eight experiments of this type, with GDP-β-S in the intracellular solution, the $t_{½}$ was 7·5 ± 1 s during a second exposure to 200 μM ATP compared with 45 ± 10 s for the first exposure. Thus, inhibiting the G proteins did not prevent the priming process, suggesting that priming is not mediated by G proteins.

Figure 5*B* shows that following activation, the current declined despite the continuous presence of 300 μM ATP (the first application of ATP is not shown for this experiment). This run-down was consistently observed and was dependent on the concentration of ATP (as discussed in an earlier section). In the example shown in Fig. 5*B*, the intracellular solution contained a non-hydrolyzable form of GTP (GTP-γ-S), which permanently activates G proteins, yet run-down was not prevented. Furthermore, the current did not recover during 10 min of wash without ATP (Fig. 5*B*, second application). In three of three additional experiments in which GTP-γ-S was included in the intracellular solutions, run-down was also observed. Thus, it appears that G protein activation cannot prevent the run-down phenomenon. The mechanism of the run-down was not further studied, but could involve receptor desensitization, dephosphorylation of the receptor, or washout of a regulatory factor.

Two major types of cell-surface receptors for ATP (purinoceptors) have been characterized: G protein-coupled receptors (P2Y receptors) and ligand-gated ion channels (P2X receptors). The inability of GDP-β-S to inhibit the ATP-stimulated conductance (Fig. 5*A*) and the inability of GTP-γ-S to irreversibly activate the conductance (Fig. 5*B*), suggests that ATP directly activated an ion channel.

The conductance activated by ATP is inhibited by suramin, and is not activated by either ADP or UTP

Figure 6*A* presents a continuous current trace recorded in the standard CsCl solutions, at a holding potential of −40 mV. While ATP (100 μM) activated an inward current, neither ADP (100 μM) nor UTP (100 μM) activated any current. Similar results were observed in four of four additional experiments of this type. Bo, Zhang, Nassar, Burnstock & Schoepfer (1995) reported that $P2X_4$, the only functional cloned P2X receptor shown to be present in epithelia, is 30-fold less sensitive to ADP than to ATP. Hence the ability of a high concentration of ADP to activate a membrane conductance was investigated. Figure 6*B* shows a continuous current trace recorded at −40 mV, in an extracellular solution containing a low concentration of divalent cations (0·1 mM $BaCl_2$). While 0·03 mM ATP activated a membrane conductance, 1 mM ADP had a negligible effect. Similar results were obtained in four of four additional experiments of this type. $P2X_4$ is relatively insensitive to the non-selective competitive P2X receptor antagonist suramin. Yet, as shown in Fig. 6*C*, suramin (100 μM) inhibited the current activated by ATP (200 μM). In eleven experiments of the type shown in Fig. 6*C*, suramin (100 μM) inhibited the current activated by 200 μM ATP by 93 ± 3%. Taken together, these findings suggest that the receptor underlying the conductance characterized in the present study is not $P2X_4$, and thus it appears that the ciliated cells express a P2X receptor which has not yet been cloned.

A form of ATP uncomplexed with divalent cations activates the conductance

In preliminary experiments it was observed that the current activated by extracellular ATP was substantially reduced when $BaCl_2$ in the extracellular solution was raised from 10 to 40 mM (data not shown). Furthermore, although Ba^{2+} was found to be more permeant than TEA^+ (see above), the conductance activated by ATP was greater in an extracellular TEA-Cl solution containing 0·1 mM $BaCl_2$ in comparison to an extracellular TEA-Cl solution containing 20 mM $BaCl_2$ (Fig. 3*B*). These observations suggest that a form of ATP unbound by divalent cations was the active agonist.

In order to determine whether the purinoceptor under investigation is activated by a free or bound form of extracellular ATP, dose–response curves were constructed for a range of added ATP, using extracellular solutions containing either 0·01 or 1·58 mM $CaCl_2$ to bind the ATP.

Figure 7*A* shows the effect of different concentrations of added ATP on the holding current at −40 mV, in an extracellular solution containing 1·58 mM $CaCl_2$. Since the current activated by ATP declined with time (see Fig. 5*B*), each tested concentration of ATP was bracketed by a measurement with 100 μM added ATP. The currents were then corrected for run-down by normalizing the current activated by a given concentration of ATP to the current activated by the preceding dose of 100 μM ATP. The resulting dose–response relationships for added ATP (averaged from 10 experiments in high Ca^{2+} and 7 experiments in low Ca^{2+}) are shown in Fig. 7*B*. The dose–response relationships were fitted with the Hill equation:

$$I/I_{max} = [ATP]^n/([ATP]^n + EC_{50}{}^n), \quad (10)$$

where I is the current at a given concentration of ATP after correction for run-down, I_{max} is the maximum current after correction for run-down, EC_{50} is the concentration of ATP

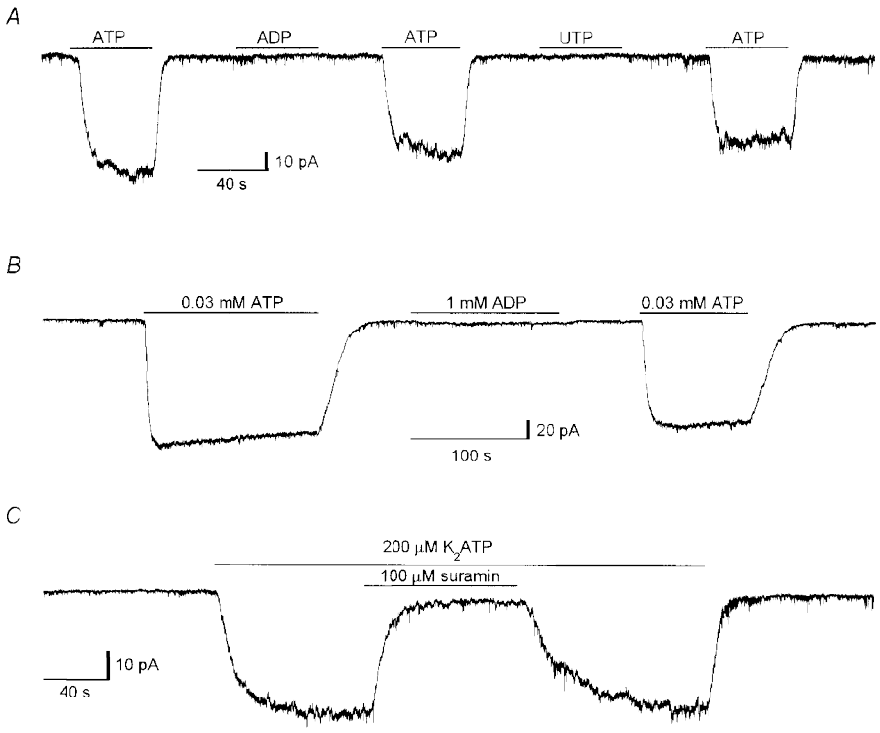

Figure 6. Neither ADP nor UTP activated a membrane conductance while suramin inhibited the conductance activated by ATP

A, continuous whole-cell current trace recorded at a holding potential of −40 mV during exposure to either ATP, ADP or UTP, all at a concentration of 100 μM. The times of exposure to each of the nucleotides are indicated by bars above the current trace. Standard intracellular and extracellular solutions. Digitized at 100 Hz, filtered at 50 Hz. Cell capacitance, 12·5 pF; series resistance, 9 MΩ. *B*, continuous whole-cell current trace recorded at a holding potential of −40 mV during exposure to either 0·03 mM ATP or 1 mM ADP. The times of exposure are indicated by bars above the current trace. The extracellular solution contained (mM): 151 CsCl, 0·1 $BaCl_2$, 5 Tes, 10 D-glucose, 1 DAP, adjusted to pH 7·4 with CsOH. Standard intracellular solution. Digitized at 100 Hz, filtered at 50 Hz. Cell capacitance, 14 pF; series resistance, 15 MΩ. *C*, continuous whole-cell current trace recorded at a holding potential of −40 mV, from a cell exposed to extracellular ATP (200 μM) for the duration indicated by the topmost bar. Suramin (100 μM) was included in the extracellular solution during the time indicated by the lower bar. Standard intracellular and extracellular solutions. Digitized at 100 Hz, filtered at 50 Hz. Cell capacitance, 12·5 pF; series resistance, 15 MΩ.

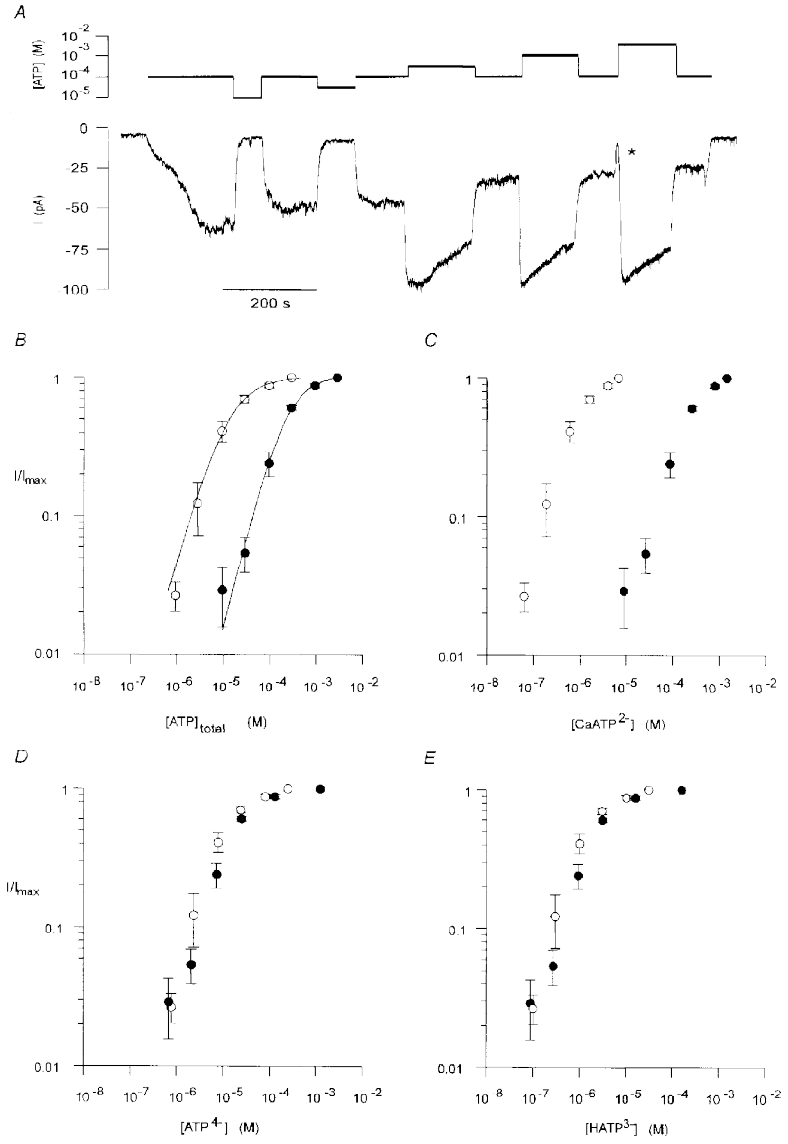

Figure 7. A form of ATP unbound by divalent cations was the active agonist

A, continuous whole-cell current trace recorded at a holding potential of −40 mV during exposure to different concentrations of extracellular ATP. The concentrations of total added ATP are indicated above the current trace on a logarithmic scale. Each tested concentration of ATP was bracketed by a measurement with 100 μM ATP. During the transition from 100 μM ATP to 3 mM ATP the cell was briefly exposed to a solution containing no ATP (*). Standard intracellular and extracellular solutions. Digitized at 500 Hz, filtered at 100 Hz. Cell capacitance, 14·5 pF; series resistance, 6·5 MΩ. *B*, reducing the total concentration of $CaCl_2$ in the extracellular solution increased the apparent effectiveness of total added extracellular ATP. Dose–response curves were constructed from current measurements similar to that shown in *A* using extracellular solutions containing either 1·58 mM $CaCl_2$ (●) or 0·01 mM $CaCl_2$ (○). For the extracellular solution containing 1·58 mM $CaCl_2$, each tested concentration of extracellular ATP was bracketed by a measurement with 100 μM ATP. The currents were corrected for run-down by normalizing the response to a given concentration of ATP to the preceding response to 100 μM ATP. Each point represents the mean (± S.E.M.) of 10 experiments. For the extracellular solution containing 0·01 mM $CaCl_2$, each point represents the mean (± S.E.M.) of 7 experiments, in which each tested concentration of extracellular ATP was bracketed by a measurement with 30 μM ATP, used to correct for run-down. The continuous lines are the least-squares fit to eqn (10) in Results. The concentrations of ATP for half-maximal activation (EC_{50}) in the high and low extracellular $CaCl_2$ were 210 and 14 μM, respectively. In both solutions the Hill coefficient (n) was 1·2. *C–E*, dose–response curves for the estimated concentrations of $CaATP^{2-}$ (*C*), ATP^{4-} (*D*), and $HATP^{3-}$ (*E*) in the experiments shown in *B*.

([ATP]) yielding a current half the maximum, and n is the Hill coefficient. Half-maximal activation (EC_{50}) shifted from 210 ± 30 to 14 ± 4 μM total added ATP when the extracellular $CaCl_2$ was reduced from 1·58 to 0·01 mM. In both low and high extracellular $CaCl_2$ concentrations the Hill coefficient (n) was estimated to be 1·2. The apparent greater concentration of ATP needed for half-maximal activation when $CaCl_2$ was raised in the extracellular solution is consistent with the active agonist being a form of ATP uncomplexed with Ca^{2+}.

To test this possibility, the concentrations of $CaATP^{2-}$, $HATP^{3-}$ and ATP^{4-} in each of the solutions were estimated (see Methods) and the dose–response curves were replotted against each of the species of ATP. It is predicted that both in low and in high extracellular Ca^{2+} the dose–response curves for the active species of ATP would be the same (overlap). Figure 7*C* shows that $CaATP^{2-}$ is unlikely to be the active species, since at all tested concentrations of $CaATP^{2-}$, the response was greater in the extracellular solution containing the low concentration of added Ca^{2+}. In contrast, the estimated dose–response curves for ATP^{4-} (Fig. 7*D*), $HATP^{3-}$ (Fig. 7*E*) and for H_2ATP^{2-} (not shown) in both low and high extracellular Ca^{2+} concentrations were similar. Since the absolute concentrations of $CaATP^{2-}$, $HATP^{3-}$ and ATP^{4-} were not accurately determined (see Methods), the dose–response curves for these species were not fitted with eqn (10). Nevertheless, the results suggest that the higher concentrations of ATP required to activate the current in extracellular solutions containing 1·58 mM Ca^{2+} resulted from the binding of Ca^{2+} to ATP. The results do not indicate, however, which charged form of ATP unbound by Ca^{2+} is the active species.

ATP uncomplexed with divalent cations activates suramin-sensitive channels in outside-out patches

To look for a possible channel underlying the ATP-induced conductance, recordings were made from outside-out patches of membrane using the standard CsCl solutions. A continuous current trace from an outside-out patch, recorded at a holding potential of −80 mV, is shown in Fig. 8*A*. The application of 200 μM ATP activated more than twenty channels in a reversible manner, giving rise to a transient inward current. Figure 8*B* plots a segment of the current record shown in Fig. 8*A* at increased time resolution from the initial phase of activation by ATP. Discrete current levels, which correspond to the activation of individual ion channels, are evident. Figure 8*C* shows an all-point histogram of the current record shown in Fig. 8*B*. Twelve peaks are visible, with an average inter-peak interval of 0·31 pA (inverse triangles in Fig. 8*C*), which corresponds to a unitary chord conductance of 3·9 pS.

To better estimate the single-channel conductance, unitary currents activated by ATP were measured at a range of negative membrane potentials. Single-channel currents were

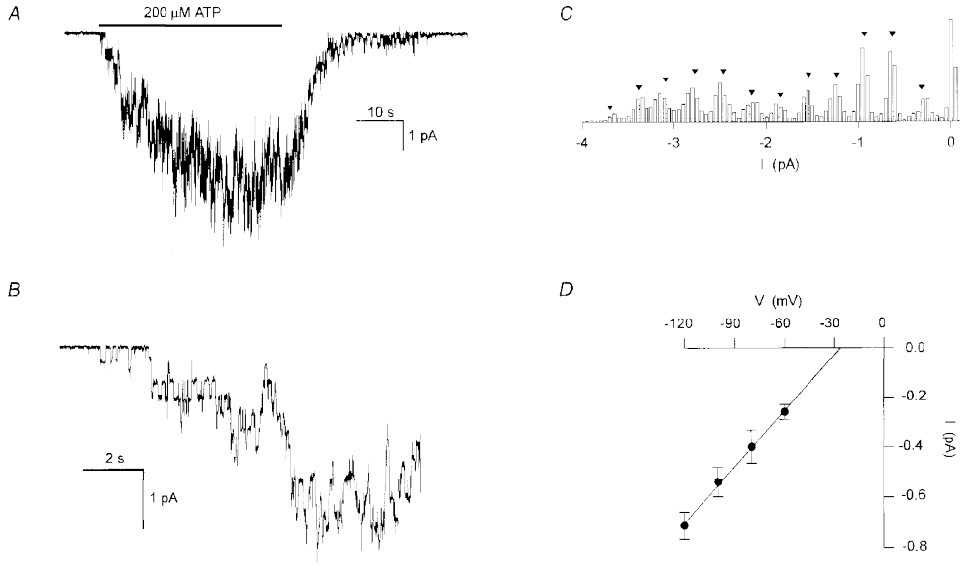

Figure 8. Ion channels were activated by extracellular ATP in outside-out membrane patches

A, continuous current trace recorded at a holding potential of −80 mV from an outside-out membrane patch. The addition of ATP (200 μM) (indicated by the bar) activated several channels. Standard intracellular and extracellular solutions. The pipette solution contained GDP-β-S (200 μM) instead of GTP. Digitized at 500 Hz, filtered at 50 Hz. The onset of channel activation by ATP is shown at increased time resolution in *B*. *C*, all-point histogram of the current trace in *B*. Bin size of 0·05 pA. The interval between the inverse triangles is 0·31 pA. *D*, current–voltage relationship for the single-channel currents activated by extracellular ATP. Each point is the mean (± S.E.M.) unitary current averaged from 4 experiments. The continuous line is a linear regression which intercepted the voltage axes at −26 mV. Same solutions as in *A*.

not measured at positive membrane potentials since the membrane patches were unstable at these potentials. It was often observed that the single-channel currents activated by ATP had two or more conductance levels (sub-levels). This is clearly seen in the third trace of Fig. 9*A*. The different conductance levels as well as the percentage of time spent in each of the conductance levels were not quantified since it was not possible to obtain outside-out patches containing a single ATP-gated channel. Hence only the maximal unitary currents were measured to estimate the main conductance level. Figure 8*D* shows the corresponding current–voltage (*I–V*) relationship of the maximal single-channel currents. Each point represents the unitary current measured at a given membrane potential averaged from four experiments. The single-channel conductance was estimated to be 7·5 pS from the slope of the *I–V* relationship. However, while similar concentrations of CsCl were used on both sides of the patch of membrane (which should give rise to a reversal potential close to 0 mV), the linear regression of the *I–V* relationship intercepted the voltage axis at approximately −26 mV. This apparent anomaly could have resulted from the inward rectifying properties of the current activated by extracellular ATP (see Fig. 2*A*). Indeed, the chord conductance at −120 mV (5·9 ± 0·5 pS) was significantly greater ($P < 0·05$) than the chord conductance at −60 mV (4·3 ± 0·5 pS), consistent with an inward-rectifying channel.

The effect of divalent cation concentration in the extracellular solution on ATP-induced channel activity was investigated in order to verify that the channels activated by ATP in outside-out membrane patches are the same channels which underlie the current measured in the whole-cell configuration.

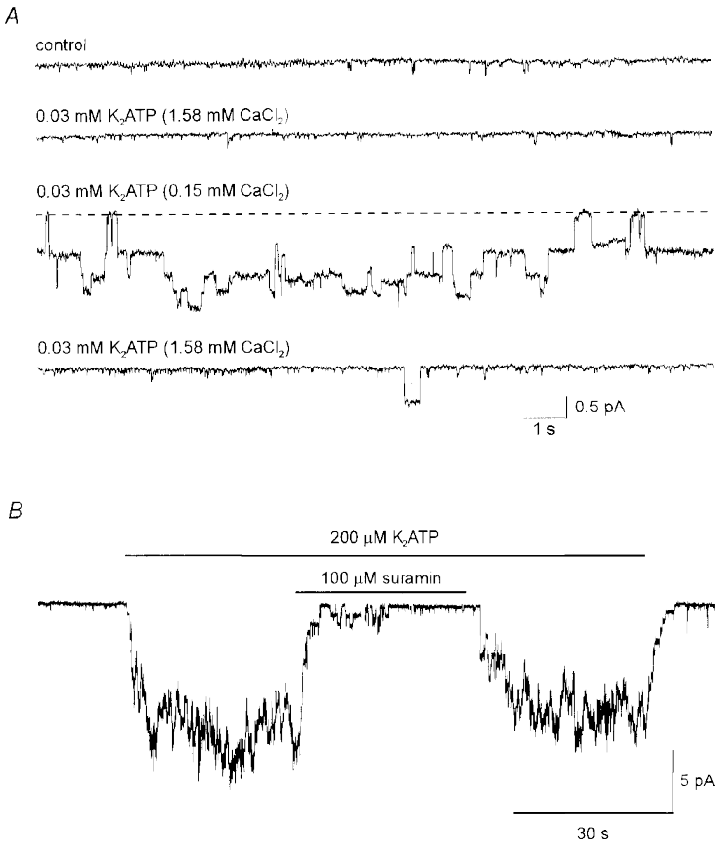

Figure 9. A form of ATP unbound by divalent cations activated suramin-sensitive channels in outside-out patches

A, ion channels were activated by reducing the $CaCl_2$ concentration in the extracellular solution from 1·58 to 0·15 mM, in the continuous presence of K_2ATP (30 μM). Current traces measured from an outside-out patch, in CsCl solutions, at a holding potential of −100 mV. The current traces were recorded from the same outside-out patch in sequence from top to bottom. The concentration of added $CaCl_2$ and added K_2ATP in the extracellular solution for each of the current traces is indicated above the current traces. Digitized at 500 Hz, filtered at 50 Hz. The dashed line indicates the current level with no channel activity for the third current trace. *B*, continuous current trace recorded from an outside-out patch of membrane at a holding potential of −120 mV. The patch was exposed to extracellular ATP (200 μM) for the duration indicated by the topmost bar. Suramin (100 μM) was included in the extracellular solution during the time indicated by the lower bar. Standard intracellular and extracellular solutions. Digitized at 500 Hz, filtered at 50 Hz.

Figure 9*A* presents four current traces measured from an outside-out patch, at a holding potential of −100 mV. The current traces were recorded in sequence from top to bottom in extracellular CsCl solutions containing different combinations of $CaCl_2$ and K_2ATP, indicated above each trace. With 1·58 mM $CaCl_2$ in the extracellular solution, 30 μM added K_2ATP did not activate ion channels (second trace). However, when the $CaCl_2$ concentration in the extracellular solution was reduced to 0·15 mM, the same concentration of added K_2ATP (30 μM) reversibly induced channel activity (downward deflections in the third current trace). This finding, which was observed in eight of eight experiments of this type, is consistent with the ion channels being gated by a form of ATP uncomplexed by Ca^{2+}.

As for the whole-cell currents (Fig. 6*C*), the channels activated by ATP (200 μM) in outside-out membrane patches were reversibly inhibited by suramin (100 μM). This is shown in Fig. 9*B* which presents a continuous current trace recorded at −120 mV from an outside-out membrane patch. In seven of seven additional outside-out membrane patches similar results were observed.

The similarity between the ATP-activated single-channel currents and the ATP-activated whole-cell currents with respect to sensitivity to suramin and to extracellular divalent cations strongly suggest that the channels characterized in the outside-out patch experiments underlie the whole-cell current activated by extracellular ATP.

DISCUSSION

The aim of the present study was to seek the pathway(s) for Ca^{2+} influx activated by extracellular ATP in rabbit airway ciliated cells by use of the patch-clamp technique (Hamill *et al.* 1981). To this end, a procedure was developed for the dissociation of ciliated cells which remained viable for several hours and were suitable for study with the patch-clamp technique. A cation-selective conductance, permeable to Ba^{2+}, was shown to be expressed by the ciliated cells. The conductance remained activated for several minutes in the continuous presence of moderate concentrations of extracellular ATP, suggesting that this conductance may be involved in maintaining the cilia at a high level of activation during prolonged exposures to ATP.

Cell-surface receptors for ATP (P2 purinoceptors) are classified into two major groups (Abbracchio & Burnstock, 1994): G protein-coupled receptors (P2Y receptors) and ligand-gated ion channels (P2X receptors). The whole-cell current characterized in this study most probably resulted from the activation of a P2X-like receptor since intracellular GDP-β-S did not inhibit the ATP-stimulated conductance (Fig. 5*A*) nor did intracellular GTP-γ-S irreversibly activate the conductance (Fig. 5*B*). Furthermore, in cell-free outside-out membrane patches, extracellular ATP activated ion channels which had a similar dependence on extracellular divalent cations (Fig. 8) as the whole-cell currents activated by ATP (Fig. 6), and were also inhibited by suramin (Fig. 9*B*). The purinoceptor characterized in this study will, therefore, be referred to as $P2X_{cilia}$.

In rabbit airway epithelium, additional P2 receptors and/or biochemical pathways are most likely involved in maintaining the cilia at an elevated level of activity for two major reasons. First, in cultures of rabbit airway epithelium, both extracellular ADP and extracellular UTP sustain the cilia at a high level of activation (N. Uzlaner & Z. Priel, unpublished observations), yet $P2X_{cilia}$ was not activated by either ADP or UTP (Fig. 6). Second, the high concentration of divalent cations (1·5 mM $CaCl_2$ and 1 mM $MgCl_2$) used in the experiments of Korngreen & Priel (1996) attenuated the current characterized in the present study by 84 ± 3 % ($n = 6$), in comparison to extracellular solutions containing 0·1 mM $BaCl_2$ and no added $CaCl_2$ or $MgCl_2$ (data not shown). Under physiological conditions, however, $P2X_{cilia}$ may contribute to Ca^{2+} influx since there are indications that the concentration of divalent cations in the airway surface fluid are lower than in the plasma (Transfiguracion, Dolman, Eidelman & Lloyd, 1995), though higher divalent cation concentrations have also been reported (Joris, Dab & Quinton, 1993).

In the conventional whole-cell configuration of the patch-clamp technique, the cytosol is replaced by the content of the patch pipette, resulting in the loss of soluble second messengers. In many cell types, extracellular ATP has been shown to release Ca^{2+} from internal stores through G protein-mediated pathway(s) (for reviews see Harden *et al.* 1995; Brake & Julius, 1996; North & Barnard, 1997). The inability of GDP-β-S to inhibit the ATP-stimulated conductance (Fig. 5*A*) suggests that the ciliated cells express at least two types of ATP receptors: a G protein-mediated receptor (P2Y receptor) which is responsible for the mobilization of Ca^{2+} from internal stores (Korngreen & Priel, 1996) and possibly underlies the effects of ADP and UTP that are observed in culture, and an ATP-gated ion channel, which mediates the currents characterized in the present study ($P2X_{cilia}$). Additional studies, using the perforated-patch whole-cell recording technique, are needed in order to identify additional pathways for ciliary activation mediated by P2 receptors for purine and pyrimidine nucleotides.

The form of ATP which gates $P2X_{cilia}$

The response to extracellular ATP was attenuated by increasing the concentration of divalent cations in the extracellular solution (Figs 7*B* and 9*A*). Such a dependence on extracellular divalent cation concentration is typically taken to indicate that the free form of ATP (ATP^{4-}) is the active agonist. However, it cannot be ruled out that the channel is gated by other forms of ATP uncomplexed with divalent cations, such as $HATP^{3-}$, H_2ATP^{2-} and $XATP^{3-}$, where X is the predominant monovalent cation in the solution (Fig. 7*D* and *E*). It is clear, however, that ATP bound by Ca^{2+} ($CaATP^{2-}$) is unlikely to gate $P2X_{cilia}$ (Fig. 7*D*). The active form of ATP could probably be determined by comparing dose–response curves for ATP

obtained in extracellular solutions containing different monovalent cations and in solutions of different acidity (pH). Such an investigation was beyond the scope of the present study.

Comparison of *P2X$_{cilia}$* to the cloned P2X purinoceptors

P2X$_{cilia}$ shares a number of features with the recently cloned P2X receptors, such as permeability to monovalent and divalent cations (Figs 2 and 3) and inward rectification of the current in symmetrical monovalent solutions (Figs 2*A* and 8*D*). One of the cloned P2X receptors, $P2X_7$, is also sensitive to the divalent cation concentration in the extracellular solution, such that increasing the divalent cation concentration in the extracellular solution attenuates the response to ATP (Surprenant, Rassendren, Kawashima, North & Buell, 1996). However, unlike *P2X$_{cilia}$*, the EC_{50} of $P2X_7$ for total extracellular ATP is unchanged by extracellular divalent cations, suggesting that it is not a free form of ATP which activates $P2X_7$. Hence, the binding sites for ATP on *P2X$_{cilia}$* and $P2X_7$ are most probably different. Other features of $P2X_7$ are also not shared by *P2X$_{cilia}$*, including the absence of inward rectification, prolonged current activation by brief exposure to ATP in low divalent solutions, and induction of cell permeabilization by long applications of ATP (Surprenant *et al.* 1996).

P2X$_{cilia}$ was shown to be cation selective (Fig. 2), as are all of the cloned P2X receptors. The ion permeability of $P2X_1$, $P2X_2$ and $P2X_7$ has been studied in detail (Evans, Lewis, Lundstrom, Buell, Surprenant & North, 1996; Surprenant *et al.* 1996). In these studies it was shown that $P2X_1$ and $P2X_2$ are 18-fold more permeable to Cs^+ than to TEA^+ and that in extracellular solutions containing physiological concentrations of divalent cations, $P2X_7$ has an ion permeability similar to that of $P2X_1$ and $P2X_2$. The estimated permeability of *P2X$_{cilia}$* to Cs^+ relative to TEA^+ (9 : 1) is, therefore, comparable to the permeability of the cloned purinoceptors. The permeability of $P2X_1$ and of $P2X_2$ to Ca^{2+} relative to Cs^+ was estimated to be 5·4 and 3·1, respectively. In the present study, the permeability of *P2X$_{cilia}$* to Ca^{2+} could not be carefully determined due to the binding of ATP by Ca^{2+}. In extracellular solutions containing 2 mM $CaCl_2$ the currents activated by 200 μM K_2ATP were too small to accurately measure reversal potentials (data not shown). Nevertheless, if the permeability of *P2X$_{cilia}$* to Ca^{2+} is equivalent to that of Ba^{2+} (Fig. 3*C*), then the permeability of *P2X$_{cilia}$* to Ca^{2+} is similar to that of $P2X_1$.

The single-channel conductance of P2X purinoceptors ranges from less than 1 pS to 60 pS (reviewed by Bean, 1992), and has been reported to be approximately 19, 21, and 9 pS for $P2X_1$, $P2X_2$ and $P2X_4$, respectively (Valera *et al.* 1994; Evans, 1996). With 151 mM Cs^+ in the bath and 155 mM Cs^+ in the pipette, the single-channel conductance of *P2X$_{cilia}$* was estimated to be 7·5 pS from the slope of the *I–V* relationship between −120 and −60 mV and estimated to be approximately 4·5 pS from the single channel current amplitudes at −60 mV. Thus, the single-channel conductance of *P2X$_{cilia}$* more closely resembles the conductance of $P2X_4$, which is the only functional cloned P2X receptor shown to be present in epithelia (Buell *et al.* 1996). Nevertheless, it is unlikely that *P2X$_{cilia}$* and $P2X_4$ are the same receptor for two major reasons. First, $P2X_4$ is most probably not activated by a free form of ATP, since micromolar concentrations of extracellular ATP activated $P2X_4$ receptors in extracellular solutions containing 110 mM $CaCl_2$ (Buell *et al.* 1996). Second, ADP was found to activate $P2X_4$ receptors (Bo *et al.* 1995; Wang, Namba, Gonoi, Inagaki & Seino, 1996) while *P2X$_{cilia}$* was insensitive to ADP (Fig. 6*B*). Taken together, the results of the present study suggest that *P2X$_{cilia}$* has, thus far, not been cloned.

The priming effect of ATP

In addition to acting as a channel activator, extracellular ATP was found to have a priming effect on *P2X$_{cilia}$* (Fig. 4). To what extent other P2X purinoceptors exhibit a similar priming response to ATP is not clear from the literature. However, Evans *et al.* (1996) typically excluded the first two applications of ATP in their study on $P2X_1$ and $P2X_2$ purinoceptors, suggesting that these purinoceptors respond differently when first exposed to ATP, in comparison to later application of ATP. In the present study, it is improbable that the slow activation during first exposure to ATP results from loss of active ATP in the perfusion system for the following reasons. (1) The perfusion time through the entire length of the tubes (from the reservoirs to the outlet) was approximately 8-fold briefer than the activation time of the current during the first exposure to ATP, at +40 mV (see Methods and Fig. 4). (2) The first application of ATP always gave rise to slow activation, even if a previous experiment was completed within less than 15 min. On the other hand, in any one experiment, rapid activation by ATP was evident 15 min after priming. (3) The rate of priming was significantly slower at a membrane potential of +40 mV in comparison to −40 mV (Fig. 4*D*), suggesting that priming is a biological phenomenon.

The priming effect of ATP is most probably not mediated by G proteins since priming persisted when the G proteins were inhibited by GDP-β-S (Fig. 5). It has recently been shown that P2X receptors can assemble as either homomultimers or heteromultimers (Lewis, Neidhart, Holy, North, Buell & Surprenant, 1995). Hence, one possible mechanism for the observed priming may be that *P2X$_{cilia}$* is a heteromultimer in which one (or more) of the subunits is not involved in the gating of the channel but serves as a regulatory subunit. A P2X receptor which could possibly be a regulatory subunit was recently cloned from rat brain (Soto, Garcia-Guzman, Karschin & Stühmer, 1996). This receptor, which is 48% identical to $P2X_5$, and is present in trachea, did not give rise to functional ATP-gated channels when expressed in *Xenopus* oocytes. If an allosteric binding site for ATP is present on *P2X$_{cilia}$*, this site would need to

be a tight-binding, low-affinity site since the effects of priming persisted for more than 15 min and since priming could be accelerated by increasing the concentration of ATP (Fig. 4*B*).

Are voltage-activated calcium channels expressed in rabbit airway ciliated cells?

The influx of Ca^{2+} in ciliated protozoans occurs primarily through voltage-gated calcium channels (for review see Tamm, 1994). In these organisms, membrane depolarization increases Ca^{2+} influx and thus regulates ciliary activity. In mucociliary cells, the pathways for Ca^{2+} influx have not been clearly determined. Recently, it was shown that mechanically induced Ca^{2+} influx in primary cell cultures of rabbit airway epithelium is blocked by nifedipine (Boitano, Woodruff & Dirksen, 1995). Furthermore, Boitano *et al.* (1995) showed that in the presence of extracellular Ca^{2+}, the calcium channel activator BAY K 8644, as well as elevated extracellular K^+ concentration, increase intracellular Ca^{2+}. These results were taken as evidence for the presence of voltage-gated calcium channels in mucociliary cells. In contrast, the present study provides direct evidence for the absence of voltage-gated calcium channels in mucociliary cells (Fig. 1*A*). This finding is in agreement with the earlier observation that calcium channel blockers such as verapamil and diltiazem did not alter Ca^{2+} influx induced by extracellular ATP and had little effect on ciliary motility in rabbit airway epithelium (Korngreen & Priel, 1996). The discrepancy between the patch-clamp data and those of Boitano *et al.* (1995) is not clear. One possible explanation may be that voltage-gated calcium channel activity was rapidly lost following the establishment of the whole-cell configuration in the freshly dissociated cells. Alternatively, cultured cells may express a pathway for Ca^{2+} influx other than voltage-gated calcium channels, which is dihydropyridine sensitive. Additional studies are clearly needed to unequivocally determine whether voltage-gated calcium channels are expressed in mucociliary cells and what role they may play in mucociliary activity and regulation.

Abbracchio, M. & Burnstock, G. (1994). Purinoceptors: are there families of P2X and P2Y purinoceptors? *Pharmacology and Therapeutics* **64**, 445–475.

Bean, B. P. (1992). Pharmacology and electrophysiology of ATP-activated ion channels. *Trends in Pharmacological Sciences* **13**, 87–90.

Benham, C. D. & Tsien, R. W. (1987). A novel receptor-operated Ca^{2+}-permeable channel activated by ATP in smooth muscle. *Nature* **328**, 275–278.

Bhagwat, S. S. & Williams, M. (1997). P2 purine and pyrimidine receptors: emerging superfamilies of G-protein-coupled and ligand-gated ion channel receptors. *European Journal of Medical Chemistry* **32**, 183–193.

Bo, X., Zhang, Y., Nassar, M., Burnstock, G. & Schoepfer, R. (1995). A P2X purinoceptor cDNA conferring a novel pharmacological profile. *FEBS Letters* **375**, 129–133.

Boitano, S., Woodruff, M. L. & Dirksen, E. R. (1995). Evidence for voltage-sensitive, calcium-conducting channels in airway epithelial cells. *American Journal of Physiology* **269**, C1547–1556.

Brake, A. J. & Julius, D. (1996). Signaling by extracellular nucleotides. *Annual Reviews of Cell and Developmental Biology* **12**, 519–541.

Buell, G., Lewis, C., Collo, G., North, R. A. & Surprenant, A. (1996). An antagonist-insensitive P_{2X} receptor expressed in epithelia and brain. *EMBO Journal* **15**, 55–62.

Butler, J. N. (1968). The thermodynamic activity of calcium ion in sodium chloride-calcium chloride electrolytes. *Biophysical Journal* **8**, 1426–1433.

Dirksen, E. R. & Sanderson, M. J. (1989). Regulation of ciliary activity in the mammalian respiratory tract. *Biorheology* **27**, 533–545.

Evans, R. J. (1996). Single channel properties of ATP-gated cation channels (P2X receptors) heterologously expressed in Chinese hamster ovary cells. *Neuroscience Letters* **212**, 212–214.

Evans, R. J., Lewis, C., Lundstrom, V. K., Buell, G., Surprenant, A. & North, R. A. (1996). Ionic permeability of, and divalent cation effects on, two ATP-gated cation channels (P2X receptors) expressed in mammalian cells. *Journal of Physiology* **497**, 413–422.

Fredholm, B. B., Abbracchio, M. P., Burnstock, G., Daly, J. W., Harden, T. K., Jacobson, K. A., Leff, P. & Williams, M. (1994). Nomenclature and classification of purinoceptors. *Pharmacological Reviews* **46**, 143–156.

Geary, C. A., Davis, C. W., Paradiso, A. M. & Boucher, R. C. (1995). Role of CNP in human airways: cGMP-mediated stimulation of ciliary beat frequency. *American Journal of Physiology* **268**, L1021–1028.

Hamill, O. P., Marty, A., Neher, E., Sakmann, B. & Sigworth, F. (1981). Improved patch-clamp techniques for high-resolution current recording from cells and cell-free membrane patches. *Pflügers Archiv* **391**, 85–100.

Harden, T. K., Boyer, J. L. & Nicholas, R. A. (1995). P_2-purinergic receptors: subtype-associated signaling responses and structure. *Annual Reviews in Pharmacology and Toxicology* **35**, 541–579.

Hille, B. (1992). *Ionic Channels of Excitable Membranes.* Sinauer Associates Inc., Sunderland, MA, USA.

Joris, L., Dab, I. & Quinton, P. M. (1993). Elemental composition of human airway surface fluid in healthy and diseased airways. *American Reviews of Respiratory Disease* **148**, 1633–1637.

Kim, Y.-K., Dirksen, E. R. & Sanderson, M. J. (1993). Stretch-activated channels in airway epithelial cells. *American Journal of Physiology* **265**, C1306–1318.

Korngreen, A. & Priel, Z. (1996). Purinergic stimulation of rabbit ciliated airway epithelia: control by multiple Ca^{2+} sources. *Journal of Physiology* **497**, 53–66.

Lansley, A. B., Sanderson, M. J. & Dirksen, E. R. (1992). Control of the beat cycle of respiratory tract cilia by Ca^{2+} and cAMP. *American Journal of Physiology* **263**, L232–242.

Levin, R., Braiman, A. & Priel, Z. (1997). Protein kinase C induced Ca^{2+} influx and sustained enhancement of ciliary beating by extracellular ATP. *Cell Calcium* **21**, 103–113.

Lewis, C. A. (1979). Ion-concentration dependence of the reversal potential and the single channel conductance of ion channels at the frog neuromuscular junction. *Journal of Physiology* **286**, 417–445.

Lewis, C., Neidhart, S., Holy, C., North, R. A., Buell, G. & Surprenant, A. (1995). Coexpression of $P2X_2$ and $P2X_3$ receptor subunits can account for ATP-gated currents in sensory neurons. *Nature* **377**, 432–435.

Lindenbaum, S. & Boyd, G. E. (1964). Osmotic and activity coefficients for symmetrical tetra-alkyl ammonium halides in aqueous solutions at 25 °C. *Journal of Physical Chemistry* **86**, 911–917.

Matsuura, H., Sakaguchi, M., Tsuruhara, Y. & Ehara, T. (1996). Activation of the muscarinic K^+ channel by P2-purinoceptors via pertussis toxin-sensitive G proteins in guinea-pig atrial cells. *Journal of Physiology* **490**, 659–671.

Mori, M., Nishizaki, T., Kawahara, K. & Okada, Y. (1996). ATP-activated cation conductance in a *Xenopus* renal epithelial cell line. *Journal of Physiology* **491**, 281–290.

Naumov, A. P., Kiselyov, K. I., Mamin, A. G., Kaznacheyeva, E. V., Kuryshev, Y. A. & Mozhayeva, G. N. (1995). ATP-operated calcium-permeable channels activated via a guanine nucleotide-dependent mechanism in rat macrophages. *Journal of Physiology* **486**, 339–347.

Neher, E. (1992). Correction for liquid junction potentials in patch clamp experiments. *Methods in Enzymology* **207**, 123–131.

North, R. A. & Barnard, E. A. (1997). Nucleotide receptors. *Current Opinion in Neurobiology* **7**, 346–357.

Ovadyahu, D., Eshel, D. & Priel, Z. (1988). Intensification of ciliary motility by extracellular ATP. *Biorheology* **25**, 489–501.

Robinson, R. A. & Stokes, R. H. (1959). *Electrolyte Solutions.* Butterworths, London, UK.

Salathe, M. & Bookman, R. J. (1995). Coupling of $[Ca^{2+}]_i$ and ciliary beating in cultured tracheal epithelial cells. *Journal of Cell Science* **108**, 431–440.

Shatkay, A. (1968). Individual activity of calcium ions in pure solutions of $CaCl_2$ and in mixtures. *Biophysical Journal* **8**, 912–919.

Soto, F., Garcia-Guzman, M., Karschin, C. & Stühmer, W. (1996). Cloning and tissue distribution of a novel P2X receptor from rat brain. *Biochemical and Biophysical Research Communications* **223**, 456–460.

Surprenant, A., Rassendren, F., Kawashima, E., North, R. A. & Buell, G. (1996). The cytolytic P_{2Z} receptor for extracellular ATP identified as a P_{2X} receptor (P_{2X7}). *Science* **272**, 735–738.

Tamm, S. (1994). Ca^{2+} channels and signaling in cilia and flagella. *Trends in Cell Biology* **4**, 305–310.

Transfiguracion, J. C., Dolman, C., Eidelman, D. H. & Lloyd, D. K. (1995). Determination of the inorganic ion composition of rat airway surface fluid by capillary electrophoresis: direct sample injection to allow multiple analyses from nanoliter volumes. *Annals of Chemistry* **67**, 2937–2942.

Valera, S., Hussy, N., Evans, R. J., Adami, N., North, R. A., Surprenant, A. & Buell, G. (1994). A new class of ligand-gated ion channel defined by P_{2X} receptor for extracellular ATP. *Nature* **371**, 516–519.

Villalón, M., Hinds, T. R. & Verdugo, P. (1989). Stimulus–response coupling in mammalian ciliated cells. Demonstration of two mechanisms of control for cytosolic $[Ca^{2+}]$. *Biophysical Journal* **56**, 1255–1258.

Wang, C. Z., Namba, N., Gonoi, T., Inagaki, N. & Seino, S. (1996). Cloning and pharmacological characterization of a fourth P2X receptor subtype widely expressed in brain and peripheral tissues including various endocrine tissues. *Biochemical and Biophysical Research Communications* **220**, 196–202.

Webb, T. E., Feolde, E., Vigne, P., Neary, J. T., Runberg, A., Frelin, C. & Barnard, E. A. (1996). The P2Y purinoceptor in rat brain microvascular endothelial cells couple to inhibition of adenylate cyclase. *British Journal of Pharmacology* **119**, 1385–1392.

Wong, L. B. & Yeates, D. B. (1992). Luminal purinergic regulatory mechanism of tracheal ciliary beat frequency. *American Journal of Respiratory Cell and Molecular Biology* **127**, 447–454.

Acknowledgements

We thank K. L. Magleby for insightful discussions and J. G. G. Borst, I. Fleidervish and M. Gutnick for helpful comments on the manuscript. This research was supported by The Israel Science Foundation founded by the Israel Academy of Sciences and Humanities – Dorot Science Foundation.

Corresponding author

S. D. Silberberg: Department of Life Sciences, Ben-Gurion University of the Negev, PO Box 653, Beer-Sheva 84105, Israel.

Email: silber@bgumail.bgu.ac.il